Marine Pollution Bulletin 186 (2023) 114369

Contents lists available at ScienceDirect

Marine Pollution Bulletin

journal homepage: www.elsevier.com/locate/marpolbul

A stable isotope assay with ^{13}C-labeled polyethylene to investigate plastic mineralization mediated by *Rhodococcus ruber*

Maaike Goudriaan [a,*], Victor Hernando Morales [a,b], Marcel T.J. van der Meer [a], Anchelique Mets [a], Rachel T. Ndhlovu [a], Johan van Heerwaarden [a], Sina Simon [c], Verena B. Heuer [c], Kai-Uwe Hinrichs [c], Helge Niemann [a,d,e,*]

[a] Department of Marine Microbiology and Biogeochemistry (MMB), Royal Netherlands Institute of Sea Research (NIOZ), 1797 SZ 't Horntje, the Netherlands
[b] Centro de Investigación Mariña, University of Vigo, Department of Ecology and Animal Biology, Biological Oceanography Group, 36319 Vigo, Spain
[c] MARUM-Center for Marine Environmental Sciences, University of Bremen, 28334 Bremen, Germany
[d] Department of Earth Sciences, Faculty of Geosciences, Utrecht University, 3584 CB Utrecht, the Netherlands
[e] CAGE–Centre for Arctic Gas Hydrate, Environment and Climate, Department of Geosciences, UiT the Arctic University of Norway, 9037 Tromsø, Norway

ARTICLE INFO

Keywords:
Microbial plastic degradation
Polyethylene biodegradation rates
Stable isotope probing
Compound specific isotope analysis
Membrane lipids
Rhodococcus ruber

ABSTRACT

Methods that unambiguously prove microbial plastic degradation and allow for quantification of degradation rates are necessary to constrain the influence of microbial degradation on the marine plastic budget. We developed an assay based on stable isotope tracer techniques to determine microbial plastic mineralization rates in liquid medium on a lab scale. For the experiments, ^{13}C-labeled polyethylene (^{13}C-PE) particles (irradiated with UV-light to mimic exposure of floating plastic to sunlight) were incubated in liquid medium with *Rhodococcus ruber* as a model organism for proof of principle. The transfer of ^{13}C from ^{13}C-PE into the gaseous and dissolved CO_2 pools translated to microbially mediated mineralization rates of up to 1.2 % yr^{-1} of the added PE. After incubation, we also found highly ^{13}C-enriched membrane fatty acids of *R. ruber* including compounds involved in cellular stress responses. We demonstrated that isotope tracer techniques are a valuable tool to detect and quantify microbial plastic degradation.

1. Introduction

Plastic pollution poses a planetary boundary threat (Arp et al., 2021; MacLeod et al., 2021). That is, waste mismanagement has led to the accumulation of plastics and their weathering products in almost any environment. This planetary-scale exposure to novel entities and chemical pollution is not readily reversible and threatens to disrupt vital Earth system processes. An estimated 1.7–4.6 % of global plastic waste ends up in the ocean (Jambeck et al., 2015), resulting in a total accumulation of 117–320 million tons (Mt) of plastic (Wayman and Niemann, 2021) in the marine environment between 1950 and 2015 (Geyer et al., 2017; Jambeck et al., 2015). However, the amount of marine plastic debris (MPD) found afloat in the oceans is estimated with 0.61–1.65 Mt (Lebreton et al., 2019), and hence much lower than the expected mass of floating MPD, a phenomenon that was coined the "ocean plastic paradox" (Thompson et al., 2004; Van Sebille et al., 2015). At least to some degree, gaps in the global MPD budget are related to inaccurate quantification of floating and submerged plastics. For example, surface trawls underestimate the total amount of MPD (Kooi et al., 2016; Lindeque et al., 2020; Poulain et al., 2019). Additionally, the ocean plastic paradox indicates the removal of MPD from the ocean surface (Cózar et al., 2014; Erni-Cassola et al., 2019; Kaandorp et al., 2020), but ocean plastic's fate and longevity are still not well constrained (Koelmans et al., 2017; Oberbeckmann and Labrenz, 2020). For example, the half-life of polyethylene (PE) in the marine environment is estimated to vary between 23 and 2500 years, based on extrapolations of published weathering rates from different marine environments (Chamas et al., 2020). For a better understanding of the impact of plastic pollution on the marine environment, it is thus important to unravel the fate of the missing plastic. Physical forcing through wave action and photooxidation triggered by solar radiation at the ocean surface lead to fragmentation and ultimately the generation of

* Corresponding authors at: Department of Marine Microbiology and Biogeochemistry (MMB), Royal Netherlands Institute of Sea Research (NIOZ), 1797 SZ 't Horntje, the Netherlands.
E-mail addresses: maaike.goudriaan@nioz.nl (M. Goudriaan), helge.niemann@nioz.nl (H. Niemann).

https://doi.org/10.1016/j.marpolbul.2022.114369
Received 16 February 2022; Received in revised form 10 October 2022; Accepted 11 November 2022
Available online 30 November 2022

secondary micro- and nano-plastics (Lambert and Wagner, 2016; Poulain et al., 2019; Ter Halle et al., 2016), which are not easily detectable (Chamas et al., 2020; Ter Halle et al., 2017). Photooxidation of plastics by UV-light introduces oxygen to the carbon backbone (Andrady, 2017; Fotopoulou and Karapanagioti, 2019; Gewert et al., 2015), and chain scission causes the release of smaller compounds such as hydrocarbons, oligomers and monomers (Gewert et al., 2018; Royer et al., 2018; Ward et al., 2019). Consequently, photo-oxidized plastic surfaces and degradation products are more bioavailable and may be degraded further by microbes (Romera-Castillo et al., 2018; Zhu et al., 2020).

Many plastics can be viewed as a hydrocarbon-like matrix (Jacquin et al., 2019) that contains a substantial amount of chemical energy (Oberbeckmann and Labrenz, 2020; Walters et al., 2000). Biological plastic degradation has indeed been discussed as a potential plastic sink in the marine environment (Amaral-Zettler et al., 2020; Vaksmaa et al., 2021; Zeghal et al., 2021). It is, however, a largely uncharted territory. Some microbial plastic degraders were found in terrestrial environments, eg. *Alcanivorax*, *Lysinibacillus*, *Aspergillus*, *Pseudomonas*, and *Ideonella sakaiensis* (Delacuvellerie et al., 2019; Esmaeili et al., 2013; Mohanan et al., 2020; Montazer et al., 2020; Yoshida et al., 2016) but only a few were found in marine environments (Roager and Sonnenschein, 2019; Urbanek et al., 2018). In fact, degradation rates and the influence of microbial degradation on plastic accumulation in the marine environment are unknown (Oberbeckmann and Labrenz, 2020; Rogers et al., 2020; Romera-Castillo et al., 2018; Wright et al., 2020; Zeghal et al., 2021; Zhu, 2021).

Destruction rates of MPD have been determined with in situ tests, but the results are usually ambiguous. The distinction between biotic and abiotic processes is not always clear (Oberbeckmann and Labrenz, 2020) and the methods applied in previous studies do not allow for accurate determination of microbial degradation rates (Montazer et al., 2020; Vaksmaa et al., 2021). Microbial plastic degradation consists of four stages (Amobonye et al., 2021; Jacquin et al., 2019; Oberbeckmann and Labrenz, 2020). (I) Biodeterioration can be initiated by the formation of a biofilm on the plastic surface. In this stage, the polymer undergoes superficial modification of mechanical, physical, and chemical properties. (II) During bio-fragmentation, the polymer is weathered further and fragments. (III) Once fragments are small enough and (bio)chemically modified, low molecular weight compounds can be transported into the cells. Microbes can then assimilate these during anabolic processes to build cell components such as DNA and lipids (Russell and Cook, 1995). (IV) For energy gain, the plastic-derived carbon may either be oxidized to CO_2 (mineralization) or reduced to CH_4 (Russell and Cook, 1995). In the literature, the terms degradation and mineralization are often used interchangeably, which leads to further ambiguity. In contrast to degradation rates, microbial PE mineralization rates in the marine environment have not yet been determined (Jacquin et al., 2019; Oberbeckmann and Labrenz, 2020). Previous studies have used an array of techniques to study microbial plastic degradation. For example, imaging techniques have frequently been applied, such as scanning electron microscopy (SEM), to visualize biofilms and abrasions on MPD surfaces, both of which have been interpreted as qualitative indicators of microbial plastic degradation (Eich et al., 2015; Sivan, 2011; Tribedi and Sil, 2013). Similarly, Raman (Nauendorf et al., 2016) and Fourier-transform infrared (FTIR) spectroscopy (Fontanella et al., 2010) are used to analyze chemical changes in the polymer matrix that potentially result from biodegradation. Estimates of in situ biodegradation of microplastics in marine environments was based on weight loss of plastics (Beltrán-Sanahuja et al., 2020; Chamas et al., 2020; Oberbeckmann and Labrenz, 2020; Tosin et al., 2012). Biological degradation rates of PE determined in the lab based on weight loss vary from 3.4 % of the initially added plastic after 80 days (Delacuvellerie et al., 2019), 25 % after one year (Sudhakar et al., 2008) or 7 % after 5 months (Syranidou et al., 2019). However, it is challenging to accurately determine small mass reductions. Plastic degradation rates have also been determined from microbial respiration (Eich et al., 2015; Rose et al., 2020), but oxygen consumption and CO_2 evolution rates can be ambiguous because of co-occurring degradation of carbon substrates other than plastic.

Ascertaining the impact of microbial plastic degradation in aquatic environments urgently calls for methods that (I) can provide unambiguous proof for microbial plastic degradation, and (II) allow quantifying plastic degradation at low rates (Montazer et al., 2020). Stable isotope probing (SIP) and stable isotope tracing assays have the potential to more accurately assess plastic degradation (Amobonye et al., 2021; Roager and Sonnenschein, 2019; Rogers et al., 2020; Wright et al., 2020). These methods allow to resolve substrate breakdown, formation of reaction products and growth by tracing isotope label (e.g. ^{13}C) from the plastic substrate into reaction products and cell components (e.g. DNA and lipid biomarkers) (Boschker et al., 1998; Radajewski et al., 2000). Transfer of isotope label between reaction pools can also be quantified, which in return offers the opportunity to quantify microbial kinetics (Hayes, 2004). Assimilation of plastic-derived compounds has been studied by SIP of microbial lipids and single fungal filaments (Taipale et al., 2019; Zumstein et al., 2018).

We developed a new isotope tracing/stable isotope probing approach in liquid medium, simulating conditions as found in aquatic environments, with photo-oxidized plastic to detect and quantify microbially mediated plastic degradation. In this study, we used *Rhodococcus ruber* strain C208 as a model organism to validate our method. *R. ruber* is a well-studied bacterium with the known ability to degrade hydrocarbons, aromatic compounds (Guevara et al., 2019; Kim et al., 2018) and various hydrocarbon-based plastic polymers, such as PE, polypropylene (PP) and polystyrene (PS) (Auta et al., 2018; Gilan et al., 2004; Gravouil et al., 2017; Mor and Sivan, 2008) We tested this method with PE, since it is the most produced polymer worldwide, constituting 36 % of all polymer types, and also the most commonly found plastic in the oceans (Erni-Cassola et al., 2019; Plastics Europe, 2020). Our method allows quantification of microbially mediated mineralization rates of as little as ~1 ‰ of the initially added plastic and also allows tracing plastic derived carbon into microbial biomass. This method shows great promise for improving our understanding of the role of microbial plastic degradation in the missing plastic paradox.

2. Materials and methods

2.1. Bacterial strain and pre-culture conditions

Cryopreserved *Rhodococcus ruber* (strain C208, DSM No. 45332) cultures were defrosted on ice, resuspended with sterile Milli-Q water, streaked on nutrient agar (Difco) plates, and cultured aerobically at 27 °C for 4 days. Fresh colonies were picked from the plate and sub-cultured in triplicate in 100 mL liquid nutrient broth (NB, Difco) and incubated at 28 °C in Erlenmeyer flasks (250 mL) on a rotary shaker (100 rpm) for 2 days. The mid-exponential phase of the culture was approximated, based on the doubling time of *R. ruber*, and confirmed by photo spectrometer measurements of optical density at 660 nm. Mid-exponential-phase bacterial cells were subsequently centrifuged for 10 min at 1500 rpm. To avoid carry-over of nutrients, we washed the pellet three consecutive times in 4 mL sterile minimal salt medium (MSM) (Sivan et al., 2006) (see details in Supplemental Information), followed by resuspension in MSM before inoculation.

2.2. Bottle setups

To compare the effect of immersion of plastics relative to floating plastics on degradation rates, we tested a newly designed bottle setup (in which plastic particles remain submerged; Fig. S1) against a regular incubation bottle (control; plastics remain afloat). For kinetic experiments, we set up parallel incubations in quadruplet with both bottle types to compare the two systems: (I) 100 mL borosilicate glass lab flasks with a GL 45 neck (hereafter termed 'Standard Bottle') and (II) the same

bottles with a transparent plexiglass insert developed in house in order to maintain positively buoyant plastic particles submerged (henceforward termed 'Johan Bottle'; Fig. S1). All flasks were closed with grey bromobutyl rubber stoppers (Duran, catalogue# 292062803) to facilitate repeated headspace (HS) measurements. Plexiglass inserts were glued to the stopper with Wacker ELASTOSIL E43 RTV-1 silicone rubber glue and covered with a gauze (1 μm mesh size) at the other end, thus creating a gaseous HS separated from particles in the aqueous phase, while still allowing gas exchange between medium and headspace. Magnetic stirrers (5 mm in length) were joined to both sides of the gauze to remove potential biofilm prior to gas measurements by placing the bottles on a stirrer plate for 2 min.

2.3. Determination of mineralization kinetics

We carried out kinetic tests in quadruple in closed bottles with MSM and with ^{13}C-labeled polyethylene powder (poly(ethylene-$^{13}C_2$), 99 atom-% ^{13}C-labeled, Sigma Aldrich, Batch#: MBBC2556, white powder, granule diameter ≪1 mm, ID confirmed by FT-IR) as the sole added carbon source. Since photochemical alteration of floating plastic is an important process at the sea surface that likely influences microbial plastic interactions, we treated the PE with UV-light to simulate natural solar light. This is commonly done in other studies on microbial plastic degradation, too (Arp et al., 2021; Gerritse et al., 2020; Rose et al., 2020; Rummel et al., 2021; Sivan et al., 2006; Wright et al., 2020). For this, the ^{13}C-PE was irradiated with ultraviolet A and B light for 75 h prior to setting up incubations. Subsequently, the polymer particles were sterilized (30 min in 70 % ethanol) and air dried in a laminar flow cabinet. For each setup we added 2 mg of labeled polymer to bottles with ~90 mL MSM, leaving a gaseous HS of ~42 mL. We then inoculated each biotic incubation with 250 μL of the pre-washed *R ruber* inoculum (ca. 8.2 × 10^8 colony-forming units (CFU) mL^{-1}). For both bottle types, 4 extra inoculated bottles were immediately fixed by adding 1 mL of saturated mercury-chloride ($HgCl_2$) solution (7.4 mg mL^{-1}) and used as sterilized controls ('Johan Bottle-KC' and 'Standard Bottle-KC') for lipid biomarker measurements. Data analysis showed that the sterilized controls proved not suitable as controls for the kinetic experiments. Samples poisoned with $HgCl_2$ showed erratic changes of δ^{13}C-values of the $CO_{2(HS)}$ and a decrease in dissolved inorganic carbon (DIC) concentrations (data not shown). At present, we can only speculate how $HgCl_2$ interfered with the PE polymer and carbonate system (see Supplemental Information). As controls for the kinetic experiments, we set up an extra set of control incubations. We set up 4 'Standard Bottles' containing ^{13}C-PE and MSM, but these were not inoculated with *R. ruber* (abiotic control). In total, 20 bottles were incubated (Table S1).

We carried out incubations at 25 °C for ~1 month, and regularly measured the concentration of gases and the ratio of stable carbon isotopes in CO_2 accumulated in the HS. We kept bottles in an opaque box shielded from light to ascertain that we only measured microbial mineralization, without potential influence of photocatalysis on the rates. Bottles were only taken out of the box to sample the HS. We determined DIC concentrations and pH at the start and end of the incubation. Additionally, we took aliquots for lipid analyses at the end of the incubations.

2.4. Headspace measurements

During the incubations, we monitored respiration by measuring concentrations of CO_2 and CH_4, and stable carbon isotope ratios of CO_2. We used a gas chromatograph (GC) coupled to a quadrupole mass spectrometer/methanizer-flame ionization detector (GC-quadMS/FID) for concentration measurements and a GC isotope ratio monitoring MS unit (GC-irMS) for stable carbon isotope measurements. Analytical and operational details of these analyses can be found in the Supporting Information.

To compensate for the pressure changes induced by taking HS samples, and to keep incubation conditions oxygenated, we injected 2 mL of pure oxygen after every second HS measurement. In this way, dissolved oxygen concentrations remained above 135 μmol L^{-1} in the medium, as measured with a Fiber-Optic Oxygen Meter (Piccolo2) in combination with OXSP5 spot sensors (PyroScience, data not shown).

2.5. Dissolved inorganic carbon concentrations and pH measurements

CO_2 in the HS ($CO_{2(HS)}$) is in equilibrium with DIC in the aqueous phase (Millero, 1979). The total amount of CO_2 in the carbonate pool, $\sum CO_2$ (=DIC + $CO_{2(HS)}$), was used to translate the change in δ^{13}C values of $CO_{2(HS)}$ to ^{13}C-excess production, which allowed us to calculate mineralization rates. At the start and end of the incubations, we took aliquots of the incubation medium to measure DIC concentrations and pH. For this, the liquid phase of the bottles (incubation medium with microbial inoculum and plastic particles) was filtered over pre-combusted GF/F filters (Ø 25 mm) in a pre-cleaned (0.1 M HCl) syringe-filter setup. The filtrate was subsampled for DIC measurements, and DIC was measured according to Stoll et al. (2001). The pH of the liquid phase was determined with a pH meter (Mettler-Toledo Seven compact S210).

2.6. Analysis of membrane fatty acids

Lipid stable isotope probing (lipid-SIP) is the combination of lipid analysis, in this case fatty acids (FAs), with a stable isotope labelling assay. Filters for FA analysis were freeze-dried and cut into smaller pieces and extracted using a modified Bligh-Dyer protocol (Bale et al., 2019; Heinzelmann et al., 2014), after which the intact polar lipids were hydrolyzed to obtain FAs which were subsequently derivatized into FA methyl esters (FAMEs) using BF_3-methanol. FAMEs were quantified and identified, and stable carbon isotope values were determined as described previously (Bale et al., 2019; Schouten et al., 1998). Procedures for FA extraction, quantification, and measurement of δ^{13}C can be found in the Supporting Information.

From the obtained δ^{13}C values and fractional abundances of single FAs, we determined an abundance weighted average FA δ^{13} value to estimate the δ^{13}C-value of bulk biomass. We then used this bulk biomass δ^{13}C-estimate to roughly assess the amount of PE derived ^{13}C assimilated by *R. ruber* (i.e., excess ^{13}C-carbon content in the bacterial particulate biomass; ^{13}Cex-bac-POM). Further details of the calculations can be found in the Supporting Information. As a control for the FA analysis, we used biomass of sterilized control experiments (Johan Bottle-KC and Standard Bottle-KC).

2.7. Calculation of PE mineralization rates

Degradation of the ^{13}C-labeled PE substrate leads to a transfer of ^{13}C-label into the product pool, such as the terminal oxidation product CO_2 and biomass. Transformation kinetics of labeled substrates can be used to determine microbial mineralization rates of plastics (Hama et al., 1993). We traced the ^{13}C-label from >99 % ^{13}C-labeled PE into CO_2 to determine PE mineralization kinetics according to the following reaction:

$$[C_2H_4]_{(n)} + 3n\ O_2 \rightarrow 2n\ (CO_2 + H_2O) \quad (1)$$

At the start of the incubations, the setups already contained CO_2 and DIC in the incubation medium, and organic matter from the microbial inoculum, all of which contain a mix of ^{12}C and ^{13}C. As a consequence, the measured CO_2/DIC pools of the incubations contain ^{13}C from PE mineralization as well as an admixture of residual ^{13}C and ^{12}C. To determine microbially mediated rates, we quantified the total amount of ^{13}C in $\sum CO_2$ originating from PE mineralization, produced in excess to the amount of ^{13}C originating from background processes. The absolute amount of ^{13}C in a given carbon pool can be determined from the

fractional abundance of ^{13}C (^{13}F) and the total amount of carbon in the given pool (Hayes, 2004).

Since, in the carbonate system, DIC is in isotopic equilibrium with $CO_{2(HS)}$, any change in ^{13}F-$CO_{2(HS)}$ corresponds to an equal change in ^{13}F in the DIC pool (albeit with a relatively small but constant offset due to equilibrium isotope effects (Zeebe and Wolf-Gladrow, 2001)). Hence, changes in ^{13}F in the $\sum CO_2$ pool can be determined from changes in ^{13}F-$CO_{2(HS)}$ and ^{13}F-$CO_{2(HS)}$ can be calculated from the $\delta^{13}C$ values of $CO_{2(HS)}$ measured by GC-irMS. We calculated ^{13}F values according to the principles published by Hayes (2004), as presented in the Supplemental Information.

We assumed that changes in ^{13}F in $\sum CO_2$ were caused by admixture of ^{13}C from PE-mineralization, and potentially ongoing background reactions will not change ^{13}F substantially (note that this does not account for minor isotope fractionation related to microbial mineralization of necro-mass or PE-derived carbon). Therefore, the change in ^{13}F-$\sum CO_2$ during the time course of the incubation and the total amount of carbon in the $\sum CO_2$ pool translates to a ^{13}C-excess production ($^{13}C_{ex}$):

$$^{13}C_{ex} = \left[\left(^{13}F\text{-}\sum CO_2\right)_{tn} - \left(^{13}F\text{-}\sum CO_2\right)_{t0}\right] \times \left(\sum CO_2\right)_{tn} \quad (2)$$

where $(^{13}F\text{-}\sum CO_2)_{tn}$ and $(^{13}F\text{-}\sum CO_2)_{t0}$ denote the fractional abundance of ^{13}C in the $\sum CO_2$-pool at the end and start of the incubation, respectively, and $(\sum CO_2)_{tn}$ the total amount of carbon in the $\sum CO_2$ pool at the end of the incubation.

Since DIC values were only available for the start and end point of the incubation, $^{13}C_{ex}$ could only be determined quantitatively for the endpoint. To estimate the $^{13}C_{ex}$ production over time, we used a modeling approach to assess $\sum CO_2$ for intermediate time points. We based this model on Henry's law and assumed that speciation of gaseous versus dissolved CO_2 progressed linearly, as explained in the Supporting Materials. From the measured and modeled values of $\sum CO_2$, we determined $^{13}C_{ex}$ based on $\delta^{13}C$-values of $CO_{2(HS)}$, which were measured regularly during the time course of the incubation. For further rate calculations, we corrected $^{13}C_{ex}$ in the experiments for abiotic $^{13}C_{ex}$ ($^{13}C_{ex}$(abiotic)) to obtain net ^{13}C excess production ($^{13}C_{ex}$(net)), as expressed in Eq. (3):

$$^{13}C_{ex}(\text{net}) = {}^{13}C_{ex}(\text{life}) - {}^{13}C_{ex}(\text{abiotic}) \quad (3)$$

The $^{13}C_{ex}$(net) was then used to calculate the amount of PE mineralized during the incubations. The rate of microbial mineralization of PE (in μg month^{-1}) is then defined as the net amount of PE degraded during the incubation divided by the duration of the incubation.

3. Results and discussion

3.1. Concentration and stable carbon isotope composition of headspace CO_2

Over the course of the incubations (ca. 1 month), we frequently measured the $CO_{2(HS)}$ concentrations of the Standard Bottle, Johan Bottle, and abiotic control. The CO_2 concentrations in the Johan Bottle at day 0 of the incubation were ~ 150 ppm higher compared to the Standard Bottle. Yet, in both biotic incubations, the CO_2 concentrations increased over time by ~250 ppm (Fig. S2A). During the first 5 days of incubation, $CO_{2(HS)}$ concentrations in all incubation types were behaving erratically/random, which is also evident from the variation between the replicates. We attribute the erratic pattern to equilibration of the gas with the aqueous phase. Nevertheless, there is a consistent trend of increasing $CO_{2(HS)}$ concentrations over time during both biotic incubations and for all replicates, mainly in the first 10–15 days. In the abiotic control, the CO_2 concentration at the start (day 0) of the incubation was ~780 ppm higher compared to the biotic incubations. However, in contrast to the biotic incubations, CO_2 concentrations in the abiotic control remained constant over time in all four replicates. Thus, CO_2 production in the biotic incubations originated from biological activity and indicates biological plastic mineralization.

The $\delta^{13}C$-CO_2 values for the biotic incubations also showed a major increase (to 462 ‰ (Johan Bottle) and to 794 ‰ (Standard Bottle); Fig. S2B; Table S2). We observed the strongest increase of $\delta^{13}C$-CO_2 values in the first 10–12 days of the incubation, after which the rate of increase levelled off. The abiotic control showed a different, almost linearly increasing trend in the $\delta^{13}C$-CO_2-values, but the total increase (~120 ‰) was much smaller than in the biotic incubations. Additionally, maximum $\delta^{13}C$-CO_2-values remained below 160 ‰, several hundred ‰ lower than biotic incubations. The relatively limited increase in $\delta^{13}C$-values of $CO_{2(HS)}$ in the abiotic control can be explained by ongoing radical reactions after the initiation of photooxidation (Gewert et al., 2015; Royer et al., 2018; Ward et al., 2019), which potentially leads to prolonged ^{13}C-DIC/CO_2 leaching from the polymer particles even after exposure to the UV-source was stopped.

3.2. pH and dissolved inorganic carbon of the incubation medium

The pH and DIC concentrations were measured at the start and end of the incubations. We adjusted the pH to 8.0 at the start in all treatments. Throughout all incubations, pH values slightly dropped by 0.3 pH units (Table S2), due to microbial CO_2 production; in the abiotic control, this can be attributed to the ongoing leaching of CO_2 and photooxidation products into the medium. Similar to $CO_{2(HS)}$ concentrations, we found strong increases in DIC concentrations in the biotic incubations, 3-fold in the Standard Bottle and 4-fold in the Johan Bottle. In contrast, concentrations in the abiotic control increased only 2-fold (Table S2). Corrected for the volumes of liquid (~90 mL) and gaseous HS (~42 mL) in both bottle setups, the change in $CO_{2(HS)}$ and liquid phase DIC concentrations translate to the production of total inorganic carbon ($\sum CO_2$) of 14.2 μmol (Standard) and 22.3 μmol (Johan Bottle) in the biotic incubations, contrasting with the 5.2 μmol in the abiotic control (Table S2). The higher increase of $\sum CO_2$ in the biotic incubations corresponds to a similarly higher increase in $\delta^{13}C$-values of $CO_{2(HS)}$ when compared to abiotic control. The transfer of ^{13}C from the isotopically labeled PE substrate to the $\sum CO_2$ pool was thus higher in biotic incubations, which provides unambiguous evidence for microbially mediated mineralization of PE-derived carbon. Our results corroborate earlier observations of the capability of *R. ruber* to degrade PE. For example, UV pre-treated PE was degraded by *R. ruber* in laboratory-based experiments, as demonstrated by FTIR analyses of the PE film (Gilan et al., 2004), determined by gravimetric weight loss (Nanda et al., 2010; Sivan, 2011) or by a combination of gravimetry and gel permeation chromatography (GPC) (Santo et al., 2013). Other *Rhodococcus* spp. like *R. rhodochrous* also showed the capability to degrade PE, as shown by a combination of FTIR and GPC (Bonhomme et al., 2003).

3.3. Microbially mediated plastic degradation and microbial mineralization rates

3.3.1. Net excess production of $\sum {}^{13}CO_2$

We calculated the fractional abundance of ^{13}C (^{13}F) for each timepoint from the obtained $\delta^{13}C$-CO_2 values, as described in the Supplemental Information. We than determined the absolute $^{13}C_{ex}$ from ^{13}F and the total amount of inorganic carbon in $\sum CO_2$ according to Eq. (2). At the end of biotic incubations, $^{13}C_{ex}$ amounted to 0.15 μmol (Johan Bottle) and 0.18 μmol (Standard Bottle) (Fig. 1; Fig. S3). We also found ^{13}C excess production ($^{13}C_{ex}$) in the abiotic control, which was presumably related to perpetuated CO_2 production after photooxidation (Gewert et al., 2018; Romera-Castillo et al., 2018; Ward et al., 2019). However, this was significantly lower than in the biotic incubations ($p \leq 0.01$ and $p = 0.0004$, *t*-test) (Fig. S3). For further rate calculations, we corrected $^{13}C_{ex}$ in the biotic controls for background processes in the experiments (Eq. (3)) against the abiotic control to obtain $^{13}C_{ex}$(net). We found that $^{13}C_{ex}$(net) was 0.132 μmol for the Johan Bottle and to 0.159

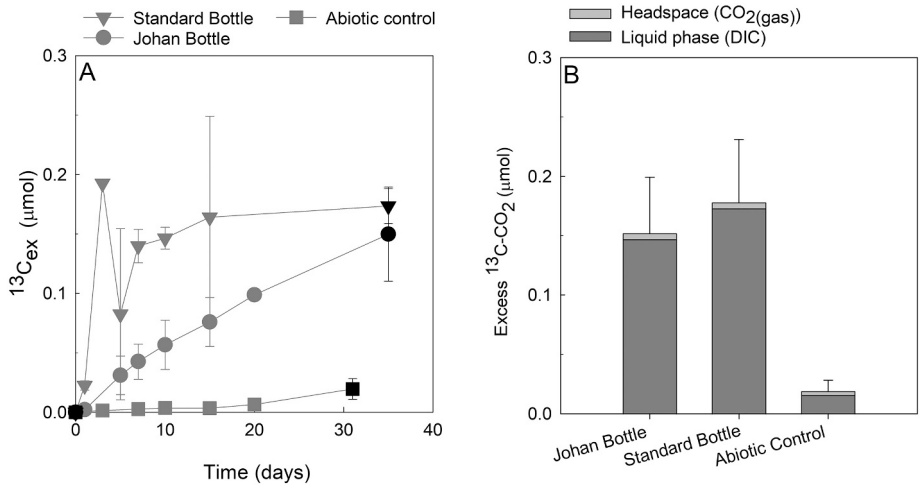

Fig. 1. Panel A: Net excess labeled CO_2 production as calculated by Eq. (3). Black symbols denote $^{13}C_{ex}$-values calculated from measurements of DIC and CO_2 values, while grey symbols denote values based on modelled $\sum CO_2$. Data are presented as averages ± standard deviation ($n = 4$). Panel B: Excess of $^{13}CO_2$ (light grey) and ^{13}C-DIC (dark grey) produced over the course of the incubation (35 days). Stacked bars represent total ^{13}C-excess production ± standard deviation (n = 4).

µmol for the Standard Bottle (Table 1).

We calculated the $^{13}C_{ex}$ at intermediate timepoints from the modelled $\sum CO_2$ values to assess the $^{13}C_{ex}$(net) production over time. In the Johan Bottle, we observed a steady $^{13}C_{Ex}$ increase, while the Standard Bottle showed some plateauing in the later phase of the incubation (Fig. 1). Similar trends of decreasing CO_2 production rates in incubations with *Rhodococcus rhodochrous* and PE were reported previously by Rose et al. (2020). The apparent plateauing in $^{13}C_{ex}$, reflects a steady state of the culture and several possible explanations for this can be found in (a combination of) the following processes, which are all inherent to microbial physiology of *R. ruber* in microcosm incubations: (I) Microbes can mainly degrade photooxidation products of PE (Romera-Castillo et al., 2018; Zhu, 2021) (i.e., nano-plastics, oligomers, monomers, and short-chain compounds that can also contain functional groups (Gewert et al., 2015)). These are probably easier to metabolize than the virgin polymer (Wayman and Niemann, 2021) and as a consequence, *R. ruber* could become carbon limited once photooxidation products are depleted. Rose et al. (2020) also suggested that decreasing CO_2 production in incubations with *Rhodococcus rhodochrous* and PE were related to limitations in bioavailable carbon. (II) Another potential process leading to plateauing of CO_2 production is that *R. ruber* grows either in biofilms or flocculant aggregates (Gilan et al., 2004; Sivan et al., 2006). Once all available surface on plastic particles is covered with a *R. ruber* biofilm, the PE-related metabolic activity of the culture can no longer increase and thus the transformation rate of ^{13}C-PE to ^{13}C-CO_2 remains constant. (III) In addition, biofilm formation leads to transport limitations with increasing biofilm thickness or density (Grötzschel et al., 2002), which would also limit microbial activity. (IV) Finally, we found FAs that indicate metabolic stress response (see below); potential toxicity of the plastic and/or its photodegradation could thus also lead to a decrease in metabolic activity.

Table 1
Net excess production of labeled inorganic carbon and net PE mineralization (amount during incubation and as percentage of original amount). Net values were calculated from gross ^{13}C-excess production corrected for chemical production of CO_2/DIC. Numbers represent average values ± standard deviation ($n = 4$). Note that PE mineralization rates in the Johan and Standard Bottles are not significantly different ($p \geq 0.27$, *t*-test).

	Johan Bottle	Standard Bottle
PE start (mg)	2	2
Net excess labeled inorganic carbon produced (µmol)	0.132 ± 0.052	0.159 ± 0.046
net PE mineralization (µg)	1.99 ± 0.79	2.38 ± 0.70
net PE mineralization (% $year^{-1}$)	1.04 ± 0.41	1.24 ± 0.36

3.3.2. PE mineralization rates

The net excess production of 1 unit ^{13}C-$\sum CO_2$ corresponds to the mineralization of 0.5 units of PE-monomer (Eq. (1)). With respect to the molecular weight of $^{13}C_2H_4$ of 30 g mol^{-1}, net $^{13}C_{ex}$ in the Johan Bottle (0.1532 µmol) and Standard Bottle (0.159 µmol) thus translates to respectively 1.99 µg and 2.38 µg of PE oxidized during the ~1 month time course of the experiment (Table 1). With respect to the amount of PE substrate added (2 mg), microbial mineralization thus amounts to 8.8×10^{-2} % and 10.5×10^{-2} % $month^{-1}$ (1.04 % and 1.24 % $year^{-1}$) in the Johan and Standard Bottle, respectively (Table 1).

The PE mineralization rates determined in this study only represent one of the four phases of microbial degradation, and are therefore in the order of magnitude one would expect based on overall degradation rates in literature. For example, Gilan et al. (2004) used a pure culture of *R. ruber* strain C208 and found ~8 % mass loss of initial PE during an incubation period of ~1 month. A similar approach was chosen by Sivan et al. (2006), who also used gravimetry to show that the same *R. ruber* strain was able to degrade up to 7.5 % of the initial mass of PE over the course of ~2 months. Note that comparison of our results with other work on microbial PE degradation rates needs to be done with caution. Most studies present overall degradation rates, for example by measuring weight loss of the plastic over time. Microbial PE mineralization rates are not available in literature, which makes direct comparison of our rates with literature difficult. Also note that our rate calculations are simplified by assuming first order kinetics (a linear mineralization pattern) with constant incubation conditions during the whole incubation period and by extrapolation over a full year. Due to our focus on PE mineralization rates and the fact that we measured ^{13}C-CO_2 production rates, we exclude other microbial processes in PE degradation, i.e., bio-deterioration and bio-fragmentation that transfer PE-derived ^{13}C to the dissolved organic carbon pool. Microbial degradation apparently leads to surface abrasion (see e.g.(Mor and Sivan, 2008)). Hence, the previously used gravimetric methods might in parts be biased because of the loss of small fragments. Furthermore, it is difficult to make a comparison between different cultivation setups and methods, underscoring the need for accurate and standardized methods.

We expect that the rate of PE degradation depends on factors such as the cell density of the inoculum (more cells facilitate higher degradation rates), surface to volume ratios of incubated plastic particles (higher surface to volume ratios allow more cells to simultaneously attach to and

degrade the plastic substrate), and temperature (Montazer et al., 2020). We hypothesized that another factor influencing microbial plastic degradation is the degree of biofilm coverage of MPD, which in turn is influenced by the fraction of wetted surface (Ter Halle et al., 2016). While plastic particles with negative buoyancy will sink and thus will have a completely wetted surface, positively buoyant plastics will partially be submerged in seawater and partially exposed to air (Ter Halle et al., 2016), influencing the degree of biofilm coverage of floating plastics. As a consequence, degradation rate measurements with positively buoyant particles could be affected by the presence of a headspace that is necessary to measure gaseous CO_2. We tested this by comparing floating plastic particles exposed to the gaseous headspace directly (Standard Bottle) with particles that remain fully submerged (Johan Bottle) and found that values describing mineralization kinetics (C_{ex}(-net), PE mineralization rates or the %-mineralization of added PE) were not significantly different ($p \geq 0.27$, *t*-test). The similar performance of both bottle setups can be attributed to the water vapor saturated atmosphere in the HS of the bottles, which results in particle surfaces being wetted constantly, regardless of their immersion status in a closed bottle as used here. In addition, motion induced by the rotary shaker leads to a rolling motion of small floating particles so that all sides of the particles will successively be immersed in the water phase (Ter Halle et al., 2016). This prevents that microbial biofilms on the particle surface dry out. For small particles, we thus argue that ex-situ incubations (based on the methodological principles described here) are a valuable tool for assessing microbially mediated mineralization rates irrespective of whether these are negatively and positively buoyant.

An important objective of ongoing research is to evaluate the fate and longevity of MPD in the ocean (Wayman and Niemann, 2021). This requires meticulous measurements of sinks for ocean plastic, for instance rates of physicochemical deterioration and microbial degradation. We calculated mineralization rates from $\sum CO_2$ and δ^{13}C-CO_2 values. At a pH of ~8, at 25 °C and in equilibrium with the atmosphere, ocean and freshwater have DIC levels of ~1.2 and 1.9 mM, respectively (Orr et al., 2015). With our GC-irMS system, a difference in HS δ^{13}C-values of <5 ‰ can reliably be resolved. Theoretically, with bottle setups and incubation boundary conditions as applied here (~90 mL liquid phase containing 2 mg ^{13}C-labeled plastic, ~40 mL head space, assuming ~constant DIC, ~1 month incubation time), an increase of 5 ‰ in δ^{13}C-$\sum CO_2$ translates to a mineralization of 0.004 % month^{-1}, or 0.05 % year^{-1} of the initially added plastic (note that higher $\sum CO_2$ levels will increase the rate detection limit, since the PE mineralization product ^{13}C-CO_2 is diluted by a higher $\sum CO_2$ background). Clearly, measuring degradation rates of this magnitude with methods based on monitoring mass changes of the incubated plastic would be challenging. In addition, due to its sensitivity, our method requires relatively short incubation times in the order of days to weeks. This is especially an advantage when applying this method to study microbial plastic degradation in an environmental matrix, where long incubation times can lead to cross feeding. Because of cross feeding, ^{13}C-label will also end up in the biomass of e.g. organisms that feed on plastic degraders which in return leads to an overestimation of mineralization rates. Furthermore, our method requires only small amounts of labeled polymer, which allows for a reasonable simulation of environmental conditions in the marine realm where concentrations of buoyant plastic are also relatively low.

We quantified PE mineralization rates with a stable isotope tracer approach in a well-defined medium with *Rhodococcus ruber* as a known plastic degrader. In the past, Taipale et al. (2019) used SIP-based assays to trace ^{13}C-label from substrate PE in a lacustrine food chain. A similar approach was taken by Zumstein et al. (2018) in soil incubations to study biodegradability of ^{13}C-labeled bioplastic poly(butylene adipate-*co*-terephthalate), tracing ^{13}C-label into soil microbes and CO_2. For future studies, we suggest to not only monitor $CO_{2(HS)}$ at multiple time points but DIC, too. This allows calculating actual $^{13}C_{ex}$ production for all time points and thus improves accuracy and allows to determine degradation rates for several growth stages during the incubation. However, the comparably high volume of sample material used for DIC measurements typically requires termination of incubations for DIC measurements. This increases handling time and necessary resources. In contrast, $CO_{2(HS)}$ measurements can be conducted repeatedly over time, yielding temporal replicate measurements from single bottles. This reduces handling time and keeps the total amount of replicates relatively low. Our method is applicable for microcosm and has great potential to be used in experiments with natural samples.

3.4. Stable isotope assimilation in cellular membrane fatty acids

We traced ^{13}C from PE into microbial biomass using stable isotope probing (SIP) of fatty acids. This method allows tracing of the utilization of a specific (carbon) substrate for growth by (micro)organisms (Maxfield and Evershed, 2014; Wegener et al., 2016) and is frequently applied to unravel food web structures (Gilbert et al., 2020; Middelburg, 2014; Watzinger and Hood-Nowotny, 2019). Fatty acid distribution and associated δ^{13}C-values in both bottle types showed major differences when compared to the microbial inoculum fixed with $HgCL_2$ (sterilized controls) at the start of the incubation (Fig. 2). In both bottle setups, we found the FAs C16:1ω7 and C18:1ω8 and cyclopropyl FAs (CPFAs) cyC17:0 and cyC19:0, which were not present in the sterilized controls. Additionally, the fractional abundances of 10meC18:0 and C18:1ω9 were higher in the biotic incubations compared to the sterilized controls. In contrast, C18:0 showed a lower fractional abundance in biotic incubations versus sterilized controls in both setups. These FAs most likely emerged due to a physiological change of the bacterial cells. Our results are in accordance with previous studies showing that FA profiles from the actinomycetes *R. ruber* are dominated by C16 and C18 FAs (Gravouil et al., 2017), more specifically C16:0, C16:1ω7, C:18:0, and C18:1ω9. Additionally, previous research detected 10meC18:0 FAs in the order Actinomycetes (De Carvalho et al., 2014; Gao et al., 2021).

Similar to the high $^{13}C_{ex}$ production, compound specific stable carbon isotope analyses revealed strongly ^{13}C-enriched FAs in the biotic incubations, regardless of bottle setup (Fig. 2). δ^{13}C-values of cyC17:0, C18:1ω8 and cyC19:0 were 2000–4000 ‰ in the Johan Bottle (abundance weighted average of all FAs = 689 ‰) and higher (i.e. 2000–5500 ‰) in the Standard Bottle (abundance weighted average of all FAs = 510 ‰). This provides direct evidence that *R. ruber* C208 not only oxidized plastic-derived carbon but also assimilated it. In contrast, we could not find substantial ^{13}C-enrichment in FAs in the sterilized controls. We added the microbial inoculum to the ^{13}C-PE amended MSM and added the $HgCL_2$ ~ 30 min later, after all incubations were set up. The slight enrichment might thus be related to uptake of ^{13}C from PE during this time period.

In an attempt to approximate the amount of PE derived ^{13}C assimilated into biomass, we performed a rough estimation of $^{13}C_{ex}$-bac-POM (^{13}C-excess in bacterial particulate organic matter; see Supplementary Information). This indicates that approximately 0.77×10^{-2} and 1.06×10^{-2} μmol of ^{13}C from PE was assimilated into biomass. This is equivalent to 0.12 and 0.16 μg of degraded PE, or 0.006 % and 0.008 % of added PE in the Standard Bottle and Johan Bottle, respectively. This indicates that only a small fraction of the labeled carbon ended up in biomass. Nevertheless, note that this estimate needs to be considered with extreme caution, as we do not account for labeling uptake in other cellular compounds (e.g. sugars and proteins) and we assumed that biomass concentrations remained constant during the incubation, while the uptake of labeled material into biomass reflects growth. Therefore, we likely underestimated the labeled carbon uptake. In addition, part of the label uptake might originate from cross-feeding within the cultures. The higher variety of labeled substrates could influence the ratios in which label is assimilated in different cellular compounds, which would influence the total amount of labeled carbon detected in fatty acids at the end of the incubation. Furthermore, a large fraction of PE-derived ^{13}C has probably accumulated in the pool of dissolved organic matter,

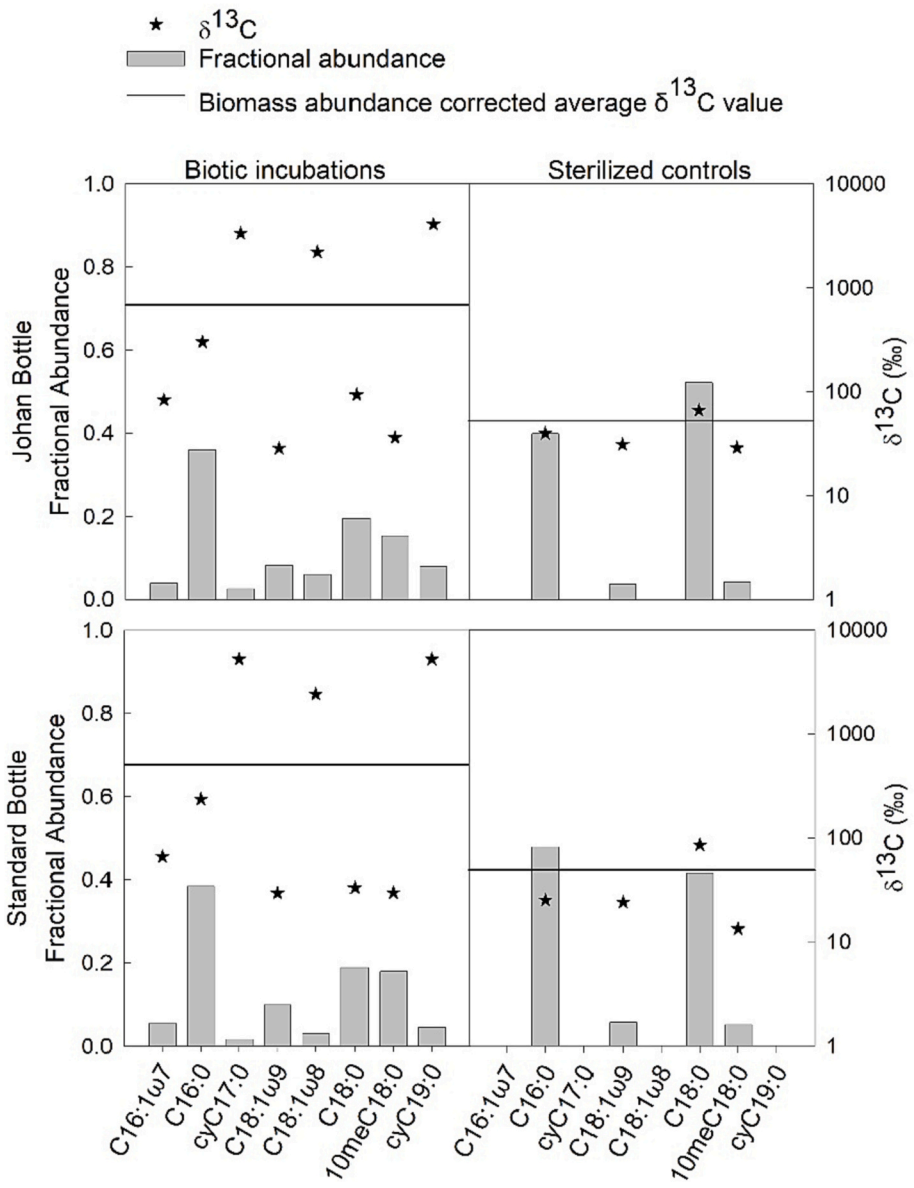

Fig. 2. Fractional abundance and $\delta^{13}C$ values of fatty acids (FAs) extracted from life incubations and sterilized controls of Johan Bottle and Standard Bottle setups. The horizontal lines represent the abundance corrected average $\delta^{13}C$ value of biomass. The FAs C16:1ω7, C18:1ω8, cyC17:0 and cyC19:0 were only present in the biotic incubations, while the cyclopropyl fatty acids (CPFAs) showed a particularly high label intensity from incorporation of carbon from labeled PE into microbial biomass.

which comprises residual photodegradation products, biofragmentation products, and metabolites from *R. ruber*. We did not analyze this pool due to absence of proper analytical protocols for well-constrained determination of $\delta^{13}C$-DOC in our laboratory facilities, since it is impossible to distinguish labeled microbial metabolites against potential leachates from the substrate that would result in a highly labeled background signal.

All FAs with high $\delta^{13}C$-values also showed a higher fractional abundance in the biotic incubations and at least some of these FAs were previously related to bacterial stress responses. In response to stressors, *Rhodococcus* species show changes in cell physiology and adaptations of the cellular membrane lipids to increase tolerance. This can result in increased unsaturation of FAs and increased content of 10meC18:0 and CPFAs (Pátek et al., 2021), as observed in *R. erythropolis* in response to increasing salt concentrations (De Carvalho et al., 2014). In case of solvent stress, the stress response decreases penetration of solvents through the inner membrane and was found to be species and solvent dependent (De Carvalho, 2019). For example, a previous study testing bioremediation potential of *R. rhodochrous* using ^{13}C-enriched C16 and C18 alkanes as carbon source, showed that the bacteria synthesized ^{13}C-enriched C16 and C19 FAs, of which the C19 FAs were probably methyl branched (Rodgers et al., 2000).

Elevated production of CPFAs in the presence of environmental contaminants is apparently a common response in several bacterial species, including *Rhodococcus* species (Murínová and Dercová, 2014). For example, elevated production of CPFAs was found in *Pseudomonas* as a membrane adaptation that increases tolerance to organic solvents and polycyclic aromatic hydrocarbons, possibly hindering accumulation of the pollutants in the cellular membrane (Pini et al., 2009). The adaptation of *R. ruber* to build up higher levels of CPFAs might be caused by hydrocarbon and hydrocarbon-like compounds that probably leach from PE as a result of UV-degradation (Gewert et al., 2018) and, possibly, microbial activity. Such compounds probably display similar adverse conditions than solvents. Cyclopropane, unsaturated, and methyl branched FAs change the packing of the lipid bilayer and lead to a higher membrane fluidity, yet CPFAs also induce a higher degree of order than unsaturated FAs (Murínová and Dercová, 2014; Poger and Mark, 2015). Additionally, CPFAs may decrease membrane permeability for protons, which aids the cell's energy conservation (Siliakus et al., 2017). Seemingly, CPFAs thus stabilize membranes against adverse conditions while promoting their fluidity. Furthermore, FA composition influences cell hydrophobicity. A decrease in membrane hydrophobicity makes it

harder for the cell to adhere to solvents while an increase in hydrophobicity facilitates cell-to-substrate attachment and promotes biofilm formation, thereby improving substrate transfer into the cell (De Carvalho, 2019).

4. Summary, conclusion and outlook

We developed and evaluated a stable isotope tracer experiment for studying the kinetics of microbial plastic mineralization in liquid medium on the lab scale. We found that our approach allows tracing isotopically labeled carbon from plastic into the mineralization product CO_2, and thus provided unambiguous proof for the mineralization of plastic-derived carbon by microbes. We measured microbial mineralization rates as low as 1 % year^{-1} of the initially added PE, and the method setup would even allow quantifying >10-fold lower rates. This is far more sensitive than determining degradation rates by gravimetric methods. Furthermore, the strong ^{13}C-labeling of membrane FAs provides evidence that PE-derived carbon supported cell growth. Our data suggest that modification of the membrane FA composition benefits *R. ruber* in media with PE and/or its photooxidation products. Despite the convenience of conducting only $CO_{2(HS)}$ measurements, our suggestion for future studies is to monitor DIC concentrations, too, to better resolve degradation kinetics. To determine gross microbial degradation rates of PE, it is furthermore crucial to fully close the carbon mass balance and to quantify the ^{13}C contents in the DOC pool and bacterial organic matter. For determining the potential of microbial species to degrade plastic, we furthermore suggest testing differential environmental conditions and substrate concentrations. The combination of ^{13}C-labeled plastic and compound specific stable isotope analysis provides an avenue for investigating microbial plastic degradation in ex-situ, and potentially, also during in-situ experiments. This method could also be applied to assess the degradation potential of plastic in complex environmental matrices (i.e., including multiple groups of microbes and different carbon substrates). For this application, it is important to consider that SIP can be affected by potential cross feeding within the microbial community. The low amount of labeled plastic needed allows for a realistic representation of the marine environment, where MPD concentrations typically are also low. Application of this method can help to constrain the role of microbial plastic degradation as a plastic sink in the marine environment.

Funding sources

This study was financed through the European Research Council (ERC-CoG Grant No. 772923, project VORTEX). VHM received funding through a postdoctoral fellowship from the Xunta de Galicia I2C program (Ref. ED481B-2018/077).

CRediT authorship contribution statement

Maaike Goudriaan: Conceptualization, Methodology, Investigation, Data Curation, Formal analysis, Writing - Original Draft and Review & Editing, Visualization. **Victor Hernando Morales:** Conceptualization, Resources, Investigation, Writing - Review & Editing. **Marcel T.J. van der Meer:** Methodology, Validation, Resources, Data Curation, Writing – Review & Editing. **Anchelique Mets:** Investigation. **Rachel T. Ndhlovu:** Methodology, Validation. **Johan van Heerwaarden:** Methodology. **Sina Simon:** Conceptualization, Methodology. **Verena B. Heuer:** Conceptualization, Methodology. **Kai-Uwe Hinrichs:** Conceptualization, Writing – Review & Editing. **Helge Niemann:** Conceptualization, Supervision, Project administration, Funding acquisition, Writing – Review & Editing.

Declaration of competing interest

The authors declare that they have no known competing financial interests or personal relationships that could have appeared to influence the work reported in this paper.

Data availability

Data will be made available on request.

Acknowledgements

The authors thank Jort Ossebaar and Ronald van Bommel for support during method development and troubleshooting in the lab. We thank Nicole Bale for advice on lipid extractions and analyses, Karel Bakker for DIC measurements and Tim de Groot for providing feedback on the manuscript as a non-expert reader.

Appendix A. Supplementary data

Experimental procedures: medium composition, GC–MS settings and procedures, IRMS settings and procedures, DIC analyses, fatty acid extraction and analyses. Mathematical reworking formulas, description determination total inorganic carbon pool intermediate time points, schematics bottle setup, summary incubations, raw data HS and DIC measurements. Supplementary data to this article can be found online at https://doi.org/10.1016/j.marpolbul.2022.114369.

References

Amaral-Zettler, L.A., Zettler, E.R., Mincer, T.J., 2020. Ecology of the plastisphere. Nat. Rev. Microbiol. https://doi.org/10.1038/s41579-019-0308-0.

Amobonye, A., Bhagwat, P., Singh, S., Pillai, S., 2021. Plastic biodegradation: frontline microbes and their enzymes. Sci. Total Environ. 759 https://doi.org/10.1016/j.scitotenv.2020.143536.

Andrady, A.L., 2017. The plastic in microplastics: a review. Mar. Pollut. Bull. 119, 12–22. https://doi.org/10.1016/j.marpolbul.2017.01.082.

Arp, H.P.H., Kühnel, D., Rummel, C., Macleod, M., Potthoff, A., Reichelt, S., Rojo-Nieto, E., Schmitt-Jansen, M., Sonnenberg, J., Toorman, E., Jahnke, A., 2021. Weathering plastics as a planetary boundary threat: exposure, fate, and hazards. Environ. Sci. Technol. https://doi.org/10.1021/acs.est.1c01512.

Auta, H.S., Emenike, C.U., Jayanthi, B., Fauziah, S.H., 2018. Growth kinetics and biodeterioration of polypropylene microplastics by bacillus sp. And rhodococcus sp. Isolated from mangrove sediment. Mar. Pollut. Bull. 127, 15–21. https://doi.org/10.1016/j.marpolbul.2017.11.036.

Bale, N.J., Irene Rijpstra, W.C., Sahonero-Canavesi, D.X., Oshkin, I.Y., Belova, S.E., Dedysh, S.N., Sinninghe Damsté, J.S., 2019. Fatty acid and hopanoid adaption to cold in the methanotroph methylovulum psychrotolerans. Front. Microbiol. 10, 1–13. https://doi.org/10.3389/fmicb.2019.00589.

Beltrán-Sanahuja, A., Casado-Coy, N., Simó-Cabrera, L., Sanz-Lázaro, C., 2020. Monitoring polymer degradation under different conditions in the marine environment. Environ. Pollut. 259 https://doi.org/10.1016/j.envpol.2019.113836.

Bonhomme, S., Cuer, A., Delort, A.M., Lemaire, J., Sancelme, M., Scott, G., 2003. Environmental biodegradation of polyethylene. Polym. Degrad. Stab. 81, 441–452. https://doi.org/10.1016/S0141-3910(03)00129-0.

Boschker, H.T.S., Nold, S.C., Wellsbury, P., Bos, D., De Graaf, W., Pel, R., Parkes, R.J., Cappenberg, T.E., 1998. Direct linking of microbial populations to specific biogeochemical processes by 13C-labelling of biomarkers. Nature 392, 801–804. https://doi.org/10.1038/33900.

Chamas, A., Moon, H., Zheng, J., Qiu, Y., Tabassum, T., Jang, J.H., Abu-Omar, M., Scott, S.L., Suh, S., 2020. Degradation rates of plastics in the environment. ACS Sustain. Chem. Eng. 8, 3494–3511. https://doi.org/10.1021/acssuschemeng.9b06635.

Cózar, A., Echevarría, F., González-gordillo, J.I., Irigoien, X., Úbeda, B., Hernández-León, S., Palma, Á.T., Navarro, S., García-de-Lomas, J., Ruiz, A., Fernández-de-Puelles, M.L., Duarte, C.M., 2014. Plastic debris in the open ocean. Proc. Natl. Acad. Sci. U. S. A. 111, 10239–10244. https://doi.org/10.1073/pnas.1314705111.

De Carvalho, C.C.C.R., 2019. Adaptation of Rhodococcus to organic solvents. In: Alvarez, H. (Ed.), Biology of Rhodococcus. Microbiology Monographs, 16. Springer, Cham, Berlin, Germany, pp. 103–135. https://doi.org/10.1007/978-3-642-12937-7_5.

De Carvalho, C.C.C.R., Marques, M.P.C., Hachicho, N., Heipieper, H.J., 2014. Rapid adaptation of rhodococcus erythropolis cells to salt stress by synthesizing polyunsaturated fatty acids. Appl. Microbiol. Biotechnol. 98, 5599–5606. https://doi.org/10.1007/s00253-014-5549-2.

Delacuvellerie, A., Cyriaque, V., Gobert, S., Benali, S., Wattiez, R., 2019. The plastisphere in marine ecosystem hosts potential specific microbial degraders including alcanivorax borkumensis as a key player for the low-density polyethylene degradation. J. Hazard. Mater. 380 https://doi.org/10.1016/j.jhazmat.2019.120899.

Eich, A., Mildenberger, T., Laforsch, C., Weber, M., 2015. Biofilm and diatom succession on polyethylene (PE) and biodegradable plastic bags in two marine habitats: early signs of degradation in the pelagic and benthic zone? PLoS One 10, 1–16. https://doi.org/10.1371/journal.pone.0137201.

Erni-Cassola, G., Zadjelovic, V., Gibson, M.I., Christie-Oleza, J.A., 2019. Distribution of plastic polymer types in the marine environment; a meta-analysis. J. Hazard. Mater. 369 https://doi.org/10.1016/j.jhazmat.2019.02.067.

Esmaeili, A., Pourbabaee, A.A., Alikhani, H.A., Shabani, F., Esmaeili, E., 2013. Biodegradation of low-density polyethylene (LDPE) by mixed culture of lysinibacillus xylanilyticus and aspergillus Niger in soil. PLoS One 8. https://doi.org/10.1371/journal.pone.0071720.

Fontanella, S., Bonhomme, S., Koutny, M., Husarova, L., Brusson, J.M., Courdavault, J.P., Pitteri, S., Samuel, G., Pichon, G., Lemaire, J., Delort, A.M., 2010. Comparison of the biodegradability of various polyethylene films containing pro-oxidant additives. Polym. Degrad. Stab. 95 https://doi.org/10.1016/j.polymdegradstab. 2010.03.009.

Fotopoulou, K.N., Karapanagioti, H.K., 2019. Degradation of various plastics in the environment. In: Handbook of Environmental Chemistry. https://doi.org/10.1007/698_2017_11.

Gao, B., Yao, H., Li, Y., Zhu, Y., 2021. Microplastic addition alters the microbial community structure and stimulates soil carbon dioxide emissions in vegetable-growing soil. Environ. Toxicol. Chem. 40, 352–365. https://doi.org/10.1002/etc.4916.

Gerritse, J., Leslie, H.A., de Tender, C.A., Devriese, L.I., Vethaak, A.D., 2020. Fragmentation of plastic objects in a laboratory seawater microcosm. Sci. Rep. 10 https://doi.org/10.1038/s41598-020-67927-1.

Gewert, B., Plassmann, M., Sandblom, O., Macleod, M., 2018. Identification of chain scission products released to water by plastic exposed to ultraviolet light. Environ. Sci. Technol. Lett. 5, 272–276. https://doi.org/10.1021/acs.estlett.8b00119.

Gewert, B., Plassmann, M.M., Macleod, M., 2015. Pathways for degradation of plastic polymers floating in the marine environment. Environ. Sci. Process. Impacts 17, 1513–1521. https://doi.org/10.1039/c5em00207a.

Geyer, R., Jambeck, J.R., Law, K.L., 2017. Production, use, and fate of all plastics ever made. Sci. Adv. 3, 25–29. https://doi.org/10.1126/sciadv.1700782.

Gilan, I., Hadar, Y., Sivan, A., 2004. Colonization, biofilm formation and biodegradation of polyethylene by a strain of Rhodococcus ruber. Appl. Microbiol. Biotechnol. 65, 97–104. https://doi.org/10.1007/s00253-004-1584-8.

Gilbert, B.M., Nachev, M., Jochmann, M.A., Schmidt, T.C., Köster, D., Sures, B., Avenant-Oldewage, A., 2020. You are how you eat: differences in trophic position of two parasite species infecting a single host according to stable isotopes. Parasitol. Res. 119, 1393–1400. https://doi.org/10.1007/s00436-020-06619-1.

Gravouil, K., Ferru-Clément, R., Colas, S., Helye, R., Kadri, L., Bourdeau, L., Moumen, B., Mercier, A., Ferreira, T., 2017. Transcriptomics and lipidomics of the environmental strain rhodococcus ruber point out consumption pathways and potential metabolic bottlenecks for polyethylene degradation. Environ. Sci. Technol. 51, 5172–5181. https://doi.org/10.1021/acs.est.7b00846.

Grötzschel, S., Köster, J., Abed, R.M.M., De Beer, D., 2002. Degradation of petroleum model compounds immobilized on clay by a hypersaline microbial mat. Biodegradation 13. https://doi.org/10.1023/A:1021263009377.

Guevara, G., Castillo Lopez, M., Alonso, S., Perera, J., Navarro-Llorens, J.M., 2019. New insights into the genome of Rhodococcus ruber strain Chol-4. BMC Genomics 20. https://doi.org/10.1186/s12864-019-5677-2.

Hama, T., Hama, J., Handa, N., 1993. In: 13C Tracer Methodology in Microbial Ecology with Special Reference to Primary Production Processes in Aquatic Environments, 13, pp. 39–83. https://doi.org/10.1007/978-1-4615-2858-6_2.

Hayes, J.M., 2004. An introduction to isotopic calculations. At. Energy.

Heinzelmann, S.M., Bale, N.J., Hopmans, E.C., Sinninghe Damsté, J.S., Schouten, S., van der Meer, M.T.J., 2014. Critical assessment of glyco- and phospholipid separation by using silica chromatography. Appl. Environ. Microbiol. 80, 360–365. https://doi.org/10.1128/AEM.02817-13.

Jacquin, J., Cheng, J., Odobel, C., Pandin, C., Conan, P., Pujo-Pay, M., Barbe, V., Meistertzheim, A.L., Ghiglione, J.F., 2019. Microbial ecotoxicology of marine plastic debris: a review on colonization and biodegradation by the "plastisphere". Front. Microbiol. 10 https://doi.org/10.3389/fmicb.2019.00865.

Jambeck, J.R., Geyer, R., Wilcox, C., Siegler, T.R., Perryman, M., Andrady, A., Narayan, R., Law, K.L., 2015. Plastic waste inputs from land into the ocean. Science (80-.) 347. https://doi.org/10.1126/science.1260352.

Kaandorp, M.L.A., Dijkstra, H.A., Van Sebille, E., 2020. Closing the Mediterranean marine floating plastic mass budget: inverse modeling of sources and sinks. Environ. Sci. Technol. 54 https://doi.org/10.1021/acs.est.0c01984.

Kim, D., Choi, K.Y., Yoo, M., Zylstra, G.J., Kim, E., 2018. Biotechnological potential of rhodococcus biodegradative pathways. J. Microbiol. Biotechnol. 28, 1037–1051. https://doi.org/10.4014/jmb.1712.12017.

Koelmans, A.A., Kooi, M., Law, K.L., Van Sebille, E., 2017. All is not lost: deriving a top-down mass budget of plastic at sea. Environ. Res. Lett. 12 https://doi.org/10.1088/1748-9326/aa9500.

Kooi, M., Reisser, J., Slat, B., Ferrari, F.F., Schmid, M.S., Cunsolo, S., Brambini, R., Noble, K., Sirks, L.A., Linders, T.E.W., Schoeneich-Argent, R.I., Koelmans, A.A., 2016. The effect of particle properties on the depth profile of buoyant plastics in the ocean. Sci. Rep. 6, 1–10. https://doi.org/10.1038/srep33882.

Lambert, S., Wagner, M., 2016. Formation of microscopic particles during the degradation of different polymers. Chemosphere 161, 510–517. https://doi.org/10.1016/j.chemosphere.2016.07.042.

Lebreton, L., Egger, M., Slat, B., 2019. A global mass budget for positively buoyant macroplastic debris in the ocean. Sci. Rep. 9, 1–10. https://doi.org/10.1038/s41598-019-49413-5.

Lindeque, P.K., Cole, M., Coppock, R.L., Lewis, C.N., Miller, R.Z., Watts, A.J.R., Wilson-McNeal, A., Wright, S.L., Galloway, T.S., 2020. Are we underestimating microplastic abundance in the marine environment? A comparison of microplastic capture with nets of different mesh-size. Environ. Pollut. 265, 114721 https://doi.org/10.1016/j.envpol.2020.114721.

MacLeod, M., Arp, H.P.H., Tekman, M.B., Jahnke, A., 2021. The global threat from plastic pollution. Science (80-.). https://doi.org/10.1126/science.abg5433.

Maxfield, P.J., Evershed, R.P., 2014. Phospholipid fatty acid stable isotope probing techniques in microbial ecology. Stable Isot. Probing Relat. Technol. 37–71 https://doi.org/10.1128/9781555816896.ch3.

Middelburg, J.J., 2014. Stable isotopes dissect aquatic food webs from the top to the bottom. Biogeosciences 11, 2357–2371. https://doi.org/10.5194/bg-11-2357-2014.

Millero, F.J., 1979. The thermodynamics of the carbonate system in seawater. Geochim. Cosmochim. Acta 43. https://doi.org/10.1016/0016-7037(79)90184-4.

Mohanan, N., Montazer, Z., Sharma, P.K., Levin, D.B., 2020. Microbial and enzymatic degradation of synthetic plastics. Front. Microbiol. https://doi.org/10.3389/fmicb.2020.580709.

Montazer, Z., Najafi, M.B.H., Levin, D.B., 2020. Challenges with verifying microbial degradation of polyethylene. Polymers (Basel) 12. https://doi.org/10.3390/polym12010123.

Mor, R., Sivan, A., 2008. Biofilm formation and partial biodegradation of polystyrene by the actinomycete Rhodococcus ruber: biodegradation of polystyrene. Biodegradation 19, 851–858. https://doi.org/10.1007/s10532-008-9188-0.

Murínová, S., Dercová, K., 2014. Response mechanisms of bacterial degraders to environmental contaminants on the level of cell walls and cytoplasmic membrane. Int. J. Microbiol. https://doi.org/10.1155/2014/873081.

Nanda, S., Sahu, S., Abraham, J., 2010. Studies on the biodegradation of natural and synthetic polyethylene by Pseudomonas spp. J. Appl. Sci. Environ. Manag. 14 https://doi.org/10.4314/jasem.v14i2.57839.

Nauendorf, A., Krause, S., Bigalke, N.K., Gorb, E.V., Gorb, S.N., Haeckel, M., Wahl, M., Treude, T., 2016. Microbial colonization and degradation of polyethylene and biodegradable plastic bags in temperate fine-grained organic-rich marine sediments. Mar. Pollut. Bull. 103 https://doi.org/10.1016/j.marpolbul.2015.12.024.

Oberbeckmann, S., Labrenz, M., 2020. Marine microbial assemblages on microplastics: diversity, adaptation, and role in degradation. Annu. Rev. Mar. Sci. 12, 209–232. https://doi.org/10.1146/annurev-marine-010419-010633.

Orr, J.C., Epitalon, J.M., Gattuso, J.P., 2015. Comparison of ten packages that compute ocean carbonate chemistry. Biogeosciences 12, 1483–1510. https://doi.org/10.5194/bg-12-1483-2015.

Pátek, M., Grulich, M., Nešvera, J., 2021. Stress response in rhodococcus strains. Biotechnol. Adv. https://doi.org/10.1016/j.biotechadv.2021.107698.

Pini, C.V., Bernal, P., Godoy, P., Ramos, J.L., Segura, A., 2009. Cyclopropane fatty acids are involved in organic solvent tolerance but not in acid stress resistance in Pseudomonas putida DOT-T1E. Microb. Biotechnol. 2, 253–261. https://doi.org/10.1111/j.1751-7915.2009.00084.x.

Plastics Europe - Association of Plastic Manufacturers (Organization), 2020. Plastics – The Facts 2020, 16. PlasticEurope.

Poger, D., Mark, A.E., 2015. A ring to rule them all: the effect of cyclopropane fatty acids on the fluidity of lipid bilayers. J. Phys. Chem. B 119. https://doi.org/10.1021/acs.jpcb.5b00958.

Poulain, M., Mercier, M.J., Brach, L., Martignac, M., Routaboul, C., Perez, E., Desjean, M. C., Ter Halle, A., 2019. Small microplastics as a Main contributor to plastic mass balance in the North Atlantic subtropical gyre. Environ. Sci. Technol. 53 https://doi.org/10.1021/acs.est.8b05458.

Radajewski, S., Ineson, P., Parekh, N.R., Murrell, J.C., 2000. Stable-isotope probing as a tool in microbial ecology. Nature 403. https://doi.org/10.1038/35001054.

Roager, L., Sonnenschein, E.C., 2019. Bacterial candidates for colonization and degradation of marine plastic debris. Environ. Sci. Technol. 53, 11636–11643. https://doi.org/10.1021/acs.est.9b02212.

Rodgers, R.P., Blumer, E.N., Emmett, M.R., Marshall, A.G., 2000. Efficacy of bacterial bioremediation: demonstration of complete incorporation of hydrocarbons into membrane phospholipids from rhodococcus hydrocarbon degrading bacteria by electrospray ionization fourier transform ion cyclotron resonance mass spectrometry. Environ. Sci. Technol. 34 https://doi.org/10.1021/es990889n.

Rogers, K.L., Carreres-Calabuig, J.A., Gorokhova, E., Posth, N.R., 2020. Micro-by-micro interactions: How microorganisms influence the fate of marine microplastics. Limnol. Oceanogr. Lett. https://doi.org/10.1002/lol2.10136.

Romera-Castillo, C., Pinto, M., Langer, T.M., Álvarez-Salgado, X.A., Herndl, G.J., 2018. Dissolved organic carbon leaching from plastics stimulates microbial activity in the ocean. Nat. Commun. 9 https://doi.org/10.1038/s41467-018-03798-5.

Rose, R.S., Richardson, K.H., Latvanen, E.J., Hanson, C.A., Resmini, M., Sanders, I.A., 2020. Microbial degradation of plastic in aqueous solutions demonstrated by Co2 evolution and quantification. Int. J. Mol. Sci. 21 https://doi.org/10.3390/ijms21041176.

Royer, S.J., Ferrón, S., Wilson, S.T., Karl, D.M., 2018. Production of methane and ethylene from plastic in the environment. PLoS One 13. https://doi.org/10.1371/journal.pone.0200574.

Rummel, C.D., Lechtenfeld, O.J., Kallies, R., Benke, A., Herzsprung, P., Rynek, R., Wagner, S., Potthoff, A., Jahnke, A., Schmitt-Jansen, M., 2021. Conditioning film and early biofilm succession on plastic surfaces. Environ. Sci. Technol. 55, 11006–11018. https://doi.org/10.1021/acs.est.0c07875.

Russell, J.B., Cook, G.M., 1995. Energetics of bacterial growth: balance of anabolic and catabolic reactions. Microbiol. Rev. https://doi.org/10.1128/mmbr.59.1.48-62.1995.

Santo, M., Weitsman, R., Sivan, A., 2013. The role of the copper-binding enzyme - laccase - in the biodegradation of polyethylene by the actinomycete rhodococcus ruber. Int. Biodeterior. Biodegrad. 84, 204–210. https://doi.org/10.1016/j.ibiod.2012.03.001.

Schouten, S., Klein Breteler, W.C.M., Blokker, P., Schogt, N., Rijpstra, W.I.C., Grice, K., Baas, M., Sinninghe Damsté, J.S., 1998. Biosynthetic effects on the stable carbon isotopic compositions of algal lipids: implications for deciphering the carbon isotopic biomarker record. Geochim. Cosmochim. Acta 62. https://doi.org/10.1016/S0016-7037(98)00076-3.

Siliakus, M.F., van der Oost, J., Kengen, S.W.M., 2017. Adaptations of archaeal and bacterial membranes to variations in temperature, pH and pressure. Extremophiles. https://doi.org/10.1007/s00792-017-0939-x.

Sivan, A., 2011. New perspectives in plastic biodegradation. Curr. Opin. Biotechnol. 22, 422–426. https://doi.org/10.1016/j.copbio.2011.01.013.

Sivan, A., Szanto, M., Pavlov, V., 2006. Biofilm development of the polyethylene-degrading bacterium rhodococcus ruber. Appl. Microbiol. Biotechnol. 72, 346–352. https://doi.org/10.1007/s00253-005-0259-4.

Stoll, M.H.C., Bakker, K., Nobbe, G.H., Haese, R.R., 2001. Continuous-flow analysis of dissolved inorganic carbon content in seawater. Anal. Chem. 73, 4111–4116. https://doi.org/10.1021/ac010303r.

Sudhakar, M., Doble, M., Murthy, P.S., Venkatesan, R., 2008. Marine microbe-mediated biodegradation of low- and high-density polyethylenes. Int. Biodeterior. Biodegrad. 61, 203–213. https://doi.org/10.1016/j.ibiod.2007.07.011.

Syranidou, E., Karkanorachaki, K., Amorotti, F., Avgeropoulos, A., Kolvenbach, B., Zhou, N.Y., Fava, F., Corvini, P.F.X., Kalogerakis, N., 2019. Biodegradation of mixture of plastic films by tailored marine consortia. J. Hazard. Mater. 375 https://doi.org/10.1016/j.jhazmat.2019.04.078.

Taipale, S.J., Peltomaa, E., Kukkonen, J.V.K., Kainz, M.J., Kautonen, P., Tiirola, M., 2019. Tracing the fate of microplastic carbon in the aquatic food web by compound-specific isotope analysis. Sci. Rep. 9, 1–15. https://doi.org/10.1038/s41598-019-55990-2.

Ter Halle, A., Jeanneau, L., Martignac, M., Jardé, E., Pedrono, B., Brach, L., Gigault, J., 2017. Nanoplastic in the North Atlantic subtropical gyre. Environ. Sci. Technol. 51 https://doi.org/10.1021/acs.est.7b03667.

Ter Halle, A., Ladirat, L., Gendre, X., Goudounèche, D., Pusineri, C., Routaboul, C., Tenailleau, C., Duployer, B., Perez, E., 2016. Understanding the fragmentation pattern of marine plastic debris. Environ. Sci. Technol. 50, 5668–5675. https://doi.org/10.1021/acs.est.6b00594.

Thompson, R.C., Olson, Y., Mitchell, R.P., Davis, A., Rowland, S.J., John, A.W.G., McGonigle, D., Russell, A.E., 2004. Lost at sea: where is all the plastic? Science (80-.) 304, 838. https://doi.org/10.1126/science.1094559.

Tosin, M., Weber, M., Siotto, M., Lott, C., Innocenti, F.D., 2012. Laboratory test methods to determine the degradation of plastics in marine environmental conditions. Front. Microbiol. 3, 1–9. https://doi.org/10.3389/fmicb.2012.00225.

Tribedi, P., Sil, A.K., 2013. Low-density polyethylene degradation by pseudomonas sp. AKS2 biofilm. Environ. Sci. Pollut. Res. 20 https://doi.org/10.1007/s11356-012-1378-y.

Urbanek, A.K., Rymowicz, W., Mirończuk, A.M., 2018. Degradation of plastics and plastic-degrading bacteria in cold marine habitats. Appl. Microbiol. Biotechnol. 102, 7669–7678. https://doi.org/10.1007/s00253-018-9195-y.

Vaksmaa, A., Hernando-Morales, V., Zeghal, E., Niemann, H., 2021. Microbial degradation of marine plastics: current state and future prospects. In: Biotechnology for Sustainable Environment. https://doi.org/10.1007/978-981-16-1955-7_5.

Van Sebille, E., Wilcox, C., Lebreton, L., Maximenko, N., Hardesty, B.D., Van Franeker, J. A., Eriksen, M., Siegel, D., Galgani, F., Law, K.L., 2015. A global inventory of small floating plastic debris. Environ. Res. Lett. 10 https://doi.org/10.1088/1748-9326/10/12/124006.

Walters, R.N., Hackett, S.M., Lyon, R.E., 2000. Heats of combustion of high temperature polymers. Fire Mater. 24, 245–252. https://doi.org/10.1002/1099-1018(200009/10)24:5<245::AID-FAM744>3.0.CO;2-7.

Ward, C.P., Armstrong, C.J., Walsh, A.N., Jackson, J.H., Reddy, C.M., 2019. Sunlight converts polystyrene to carbon dioxide and dissolved organic carbon. Environ. Sci. Technol. Lett. 6 https://doi.org/10.1021/acs.estlett.9b00532.

Watzinger, A., Hood-Nowotny, R., 2019. Stable isotope probing of microbial phospholipid fatty acids in environmental samples. In: Methods in Molecular Biology. https://doi.org/10.1007/978-1-4939-9721-3_4.

Wayman, C., Niemann, H., 2021. The fate of plastic in the ocean environment – a minireview. Environmental Science Processes & Impacts. https://doi.org/10.1039/d0em00446d.

Wegener, G., Kellermann, M.Y., Elvert, M., 2016. Tracking activity and function of microorganisms by stable isotope probing of membrane lipids. Curr. Opin. Biotechnol. https://doi.org/10.1016/j.copbio.2016.04.022.

Wright, R.J., Erni-Cassola, G., Zadjelovic, V., Latva, M., Christie-Oleza, J.A., 2020. Marine plastic debris: a new surface for microbial colonization. Environ. Sci. Technol. 54, 11657–11672. https://doi.org/10.1021/acs.est.0c02305.

Yoshida, S., Hiraga, K., Takehana, T., Taniguchi, I., Yamaji, H., Maeda, Y., Toyohara, K., Miyamoto, K., Kimura, Y., Oda, K., 2016. A bacterium that degrades and assimilates PET. Science 80, 351.

Zeebe, R.E., Wolf-Gladrow, D., 2001. CO2 in Seawater: equilibrium, kinetics, isotopes. In: Chapter 1 Equilibrium, 65. Elsevier Oceanogr. Ser.

Zeghal, E., Vaksmaa, A., Vielfaure, H., Boekhout, T., Niemann, H., 2021. The potential role of marine fungi in plastic degradation – a review. Front. Mar. Sci. 8, 738877 https://doi.org/10.3389/fmars.2021.738877.

Zhu, L., Zhao, S., Bittar, T.B., Stubbins, A., Li, D., 2020. Photochemical dissolution of buoyant microplastics to dissolved organic carbon: rates and microbial impacts. J. Hazard. Mater. 383 https://doi.org/10.1016/j.jhazmat.2019.121065.

Zhu, X., 2021. The plastic cycle – an unknown branch of the carbon cycle. Front. Mar. Sci. 7, 2019–2022. https://doi.org/10.3389/fmars.2020.609243.

Zumstein, M.T., Schintlmeister, A., Nelson, T.F., Baumgartner, R., Woebken, D., Wagner, M., Kohler, H.P.E., McNeill, K., Sander, M., 2018. Biodegradation of synthetic polymers in soils: tracking carbon into CO2 and microbial biomass. Sci. Adv. 4 https://doi.org/10.1126/sciadv.aas9024.